Journal of Seismology **6:** 25–41, 2002.

Shallow seismicity, stress distribution and crustal deformation pattern in the Andaman-West Sunda arc and Andaman Sea, northeastern Indian Ocean

M. Radha Krishna & T.D. Sanu
Department of Marine Geology and Geophysics, School of Marine Sciences, Fine Arts Avenue, Cochin – 682 016, India

Received 8 February 2000; accepted in revised form 4 April 2001

Key words: seismicity, crustal deformation, apparent stress, subduction zone, Andaman – West Sunda arc, Indian Ocean

Abstract

Shallow seismicity and available source mechanisms in the Andaman–west Sunda arc and Andaman sea region suggest distinct variation in stress distribution pattern both along and across the arc in the overriding plate. Seismotectonic regionalisation indicates that the region could be divided into eight broad seismogenic sources of relatively homogeneous deformation. Crustal deformation rates have been determined for each one of these sources based on the summation of moment tensors. The analysis showed that the entire fore arc region is dominated by compressive stresses with compression in a mean direction of N23°, and the rates of seismic deformation velocities in this belt decrease northward from 5.2 ± 0.65 mm/yr near Nias island off Sumatra and 1.12 ± 0.13 mm/yr near Great Nicobar islands to as much as 0.4 ± 0.04 mm/yr north of 8°N along Andaman–Nicobar islands region. The deformation velocities indicate, extension of 0.83 ± 0.05 mm/yr along N343° and compression of 0.19 ± 0.01 mm/yr along N73° in the Andaman back arc spreading region, extension of 0.18 ± 0.01 mm/yr along N125° and compression of 0.16 ± 0.01 mm/yr along N35° in Nicobar Deep and west Andaman fault zone, compression of 0.84 ± 0.12 mm/yr N341° and extension of 0.77 ± 0.11 mm/yr along N72° within the transverse tectonic zone in the Andaman trench, N-S compression of 3.19 ± 0.29 mm/yr and an E-W extension of 1.24 ± 0.11 mm/yr in the Semangko fault zone of north Sumatra. The vertical deformation suggests crustal thinning in the Andaman sea and crustal thickening in the fore arc and Semangko fault zones. The apparent stresses calculated for all major events range between 0.1–10 bars and the values increase with increasing seismic moment. However, the apparent stress estimates neither indicate any significant variation with faulting type nor display any variation across the arc, in contrast to the general observation that the fore arc thrust events show higher stress levels in the shallow subduction zones. It is inferred that the oblique plate convergence, partial subduction of 90°E Ridge in north below the Andaman trench and the active back arc spreading are the main contributing factors for the observed stress field within the overriding plate in this region.

Introduction

The Andaman–West Sunda arc in the northeastern Indian Ocean defines a nearly 2200 km long trench slope break between the Indian plate and the SE Asia / Burma plate (Curray et al., 1979). The Andaman arc is of particular interest for its Neogene back arc spreading which presumably relates to leaky transform tectonics (Uyeda and Kanamori, 1979). The geological and tectonic history of the region is complex due to the presence of active faults / tectonic features such as the west Andaman fault in the Andaman sea, the Semangko fault in Sumatra, the Andaman-Nicobar-Nias fore arc sedimentary complex and the Neogene Andaman back arc spreading ridge (Figure 1). The Andaman basin underlying the greater part of the Andaman sea is categorised as a ‘pull-

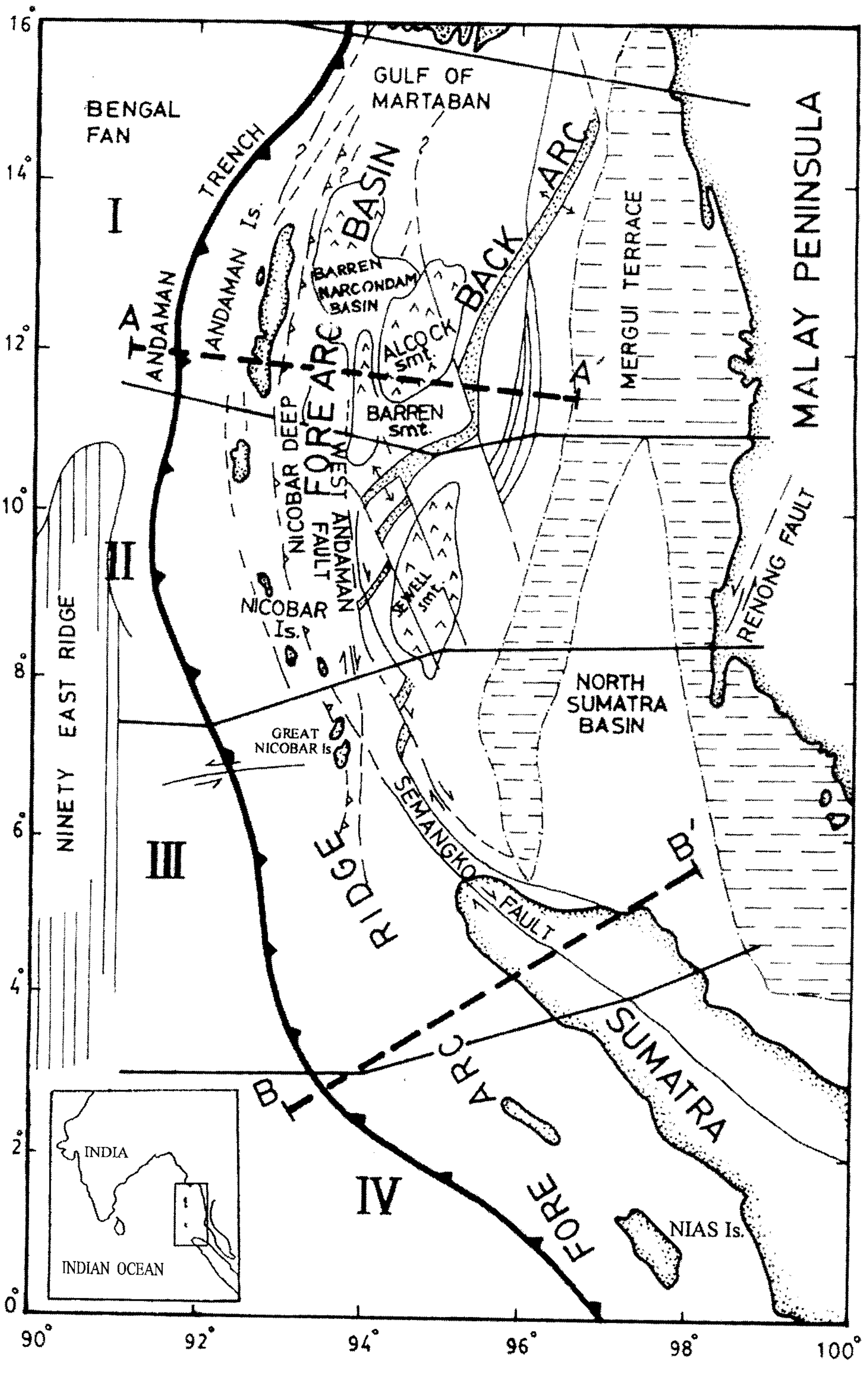

Figure 1. Tectonic and structural features of the Andaman–west Sunda arc and Andaman sea region (after Rodolfo, 1969 and Curray et al., 1979). The zones marked I–IV are the broad segmentation of the arc based on the seismicity and morphotectonic trends by Dasgupta and Mukhopadhyay (1993). Lines AA' and BB' represent sections of apparent stresses shown in Figure 6. Details are discussed in text.

apart' or 'rip-off' basin (Curray, 1987; Maung, 1987), rather than a typical back arc extensional basin. Seismic reflection studies across the trench slope from the Andaman and Sunda arc regions (Moore and Curray, 1980; Moore and Karig, 1980; Moore et al., 1980; Curray et al., 1982) indicate folding and thrusting in the accretionary prism, where a major component of convergence occurs normal to the trench axis (Curray, 1987). The structure of the Andaman-Nicobar fore arc ridge is dominated by east-dipping nappes having gentler folding in the north part of the arc as compared to tighter folding and more intense deformation within the nappes further south off Sumatra (Weeks et al., 1967; Moore and Curray, 1980).

In the present study, we utilise the hypocentral data of shallow earthquakes (h $\leq$ 70 km.) including the historical and instrumental data and a large number of focal mechanism solutions, to identify various broad seismogenic sources within Andaman–West Sunda arc and the Andaman sea, and to study the spatial variations in deformation pattern. The method is based on the calculation of apparent stresses and by summation of the moment tensor elements of shallow earthquakes.

Method and data analysis

The method of analysis followed here is one proposed by Papazachos and Kiratzi (1992) which is based on the formulations of Kostrov (1974), Molnar (1979) and Jackson and McKenzie (1988). The method was subsequently applied in seismically active regions by Papazachos et al. (1992), Kiratzi (1993), Kiratzi and Papazachos (1995) and Papazachos and Kiratzi (1996). We briefly mention the method below.

The average strain rate tensor $\dot{\epsilon}_{ij}$, which is the symmetric part of the velocity gradient tensor, is calculated by the following relation (Kostrov, 1974):

$$\dot{\epsilon}_{ij} = \frac{1}{2\mu V}\frac{\sum_{n=1}^{N} M_{ij}^{n}}{T} = \frac{1}{2\mu V}\dot{M}o\bar{F}_{ij}$$

$$i, j = 1, 2, 3 \qquad (1)$$

Where V is the deformed volume, ΣM_{ij} is the sum of the moment tensors of the earthquakes that occurred within the volume in T years, μ is the rigidity of crustal rocks, $\dot{M}o$ is the seismic moment rate, and $\bar{F}_{ij}$ is focal mechanism tensor calculated by averaging over N mechanisms, where F_{ij}^{n} is a function of strike, dip and rake of the focal mechanism (Aki and Richards, 1980).

The rate of moment release $\dot{M}o$, used in the above equation is calculated from Molnar (1979) as:

$$\dot{M}o = \frac{A}{1-B}M_{o,max}^{(1-B)} \qquad (2)$$

Where $\dot{M}_{o,max}$ is the scalar moment of the largest observed earthquake in the region and

$$A = 10^{[a+(bd/c)]} \text{and } B = b/c$$

Where a and b are the constants of the Gutenberg-Richter relation and c and d are the constants of moment–magnitude relation applicable to the area. Finally, the integrated rates of motion U_{ij} normal and parallel to the zones boundary as well as vertically are calculated by the following relations (Papazachos and Kiratzi, 1992).

$$U_{ij} = \frac{1}{2\mu l_k l_j}\dot{M}o\bar{F}_{ij}$$

$$i = 1, 2, 3 i\#j, j\#k, k\#i \qquad (3)$$

$$U_{12} = \frac{1}{2\mu l_1 l_3}\dot{M}o\bar{F}_{12} \qquad (4)$$

$$U_{i3} = \frac{1}{2\mu l_1 l_2}\dot{M}o\bar{F}_{13} \quad i = 1, 2 \qquad (5)$$

Where l_1, l_2 are length and width of the deforming zone and l_3 is the depth extent of the seismogenic layer. The reference system in equation (1), (3)–(5) is the zones local system (length/width/depth). Since $\bar{F}_{ij}$ is usually calculated in the north/east/down system, a rotation in the zone's system is necessary.

For a good number of focal mechanism solutions, the seismic moments are available from Harvard CMT catalog. These data have been utilised to calculate the apparent stresses to understand their distribution in the shallow subduction zone.

Identification of seismogenic sources and moment release rates

Seismotectonic regionalisation

Detailed studies made by several previous workers on seismicity and other geophysical data have contributed towards understanding geodynamics of the region (Weeks et al., 1967; Rodolfo, 1969; Singhval et al., 1978; Verma et al., 1978; Curray et al., 1979;

Eguchi et al., 1979; Surender Kumar, 1981; Mukhopadhyay, 1984, 1988; Rajendran and Gupta, 1989; Dasgupta, 1992; Dasgupta and Mukhopadhyay, 1993). The structural development of the arc system and the presence of active N-S faults in the Andaman sea were reported by Weeks et al. (1967), Curray et al. (1979) and Mukhopadhyay (1984). Dasgupta and Mukhopadhyay (1993) observed significant variation in the seismicity pattern related to the subducting slab from north to south in the Andaman arc region. Based on the morphotectonic setting, gravity anomaly trends and seismicity pattern, they divided the region into four broad sectors from north to south (see Figure 1). Dasgupta (1992) and Dasgupta and Mukhopadhyay (1993) observed that several structural / tectonic features such as the Andaman-Nicobar-Nias fore arc ridge, the back arc spreading center and the west Andaman fault in the Andaman sea, and the Semangko fault zone in northern Sumatra show active and well defined seismicity pattern.

Since the region under investigation is very large, it has to be divided into seismogenic sources of relatively homogeneous deformation. For this purpose, we compiled the hypocentral data of shallow earthquakes (h $\leq$ 70 km.) including the historical events from the ISC and PDE listings, Gutenberg and Richter (1954) and Rothe (1969). We considered all events of $M_s \geq 4.5$ for the present analysis. For few events, the M_s value is obtained from M_b by using M_b-M_s relation derived for the region. The magnitudes estimated by Gutenberg and Richter (1954) and Rothe (1969) are equivalent to 20-s M_s (Geller and Kanamori, 1977).The seismicity map prepared for the region is shown in Figure 2. Further, we compiled 92 focal mechanism solutions of events occurring in this region from various sources. The mechanisms are mostly compiled from quarterly reports of Harvard CMT solutions published by Dziewonski and other co-workers in PEPI, and from Dasgupta and Mukhopadhyay (1993). The source parameters of all the 92 mechanisms are listed in Table 1 and they are plotted as shown in Figure 3.

By considering the previous seismotectonic studies, a careful analysis of the seismicity map and focal mechanism solutions in correlation with various tectonic features of the region has been attempted. The analysis indicate that the Andaman arc and the surrounding regions could be divided into 8 broad seismogenic sources. The boundaries for each source are defined based on the epicentral area and the morphotectonic trends. As suggested by Papazachos and Kiratzi (1992), we have drawn rectangular shapes to these sources taking into consideration the complete record of seismicity. Most of the mechanisms in the Andaman-Nicobar-Nias fore arc region show either thrust or strike-slip faulting. This region is considered as a single seismic belt, but because of convex geometry, depending on the strike direction and trend of seismicity (Dasgupta and Mukhopadhyay, 1993), the fore arc region has been divided into 4 sources (sources 1,3,6,8). The mechanisms of events falling in these sources are utilised for estimating a single focal mechanism tensor $\bar{F}$ for the belt. The other sources include the Andaman back arc spreading region (source 2), the Nicobar Deep and west Andaman fault region (source 4), the transverse tectonic zone in the Andaman trench (source 5) and the Semangko fault zone (source 7). The length l_1, width l_2 and azimuth for each of the 8 seismogenic sources are listed in Table 2.

Moment release rates

The rates of seismic moment release for each seismogenic source can be estimated by using the equation 2 in section 2. The advantage of this formula is that the full record of seismicity can be used in any given region. The most important parameters in this calculation are a and b values of the Gutenberg–Richter relation. For estimation of these parameters, we have adopted the ‘mean value method’ used by Papazachos (1990) which was originally proposed by Milne and Davenport (1969) for earthquake risk analysis. According to this method, in a given source region, the whole time interval of available data is separated into subintervals and define for each subinterval a minimum magnitude M_{min} above which the data of the subinterval are complete. For example t and M_{min} for source 1 in Table 2 implies that data are complete for earthquakes with $M_s \geq 5.8$ from 1941–1993, for $M_s \geq 4.5$ from 1964–1993. The a and b values and total number of events used for each source are given in Table 2. The standard errors estimated for a and b values are also shown in the table.

The $M_{s,max}$ for each source is considered as the maximum magnitude ever observed for the complete record of seismicity in that source. The seismic moments of all shallow earthquakes of $M_s \geq 5.5$ and depth $\leq$ 50 km listed in Table 1 have been considered for deriving the moment–magnitude relation. Since the slope c of the moment – magnitude relation is very sensitive to errors in M_s values, by considering c equal to 1.5 as defined by Kanamori and Anderson (1975),

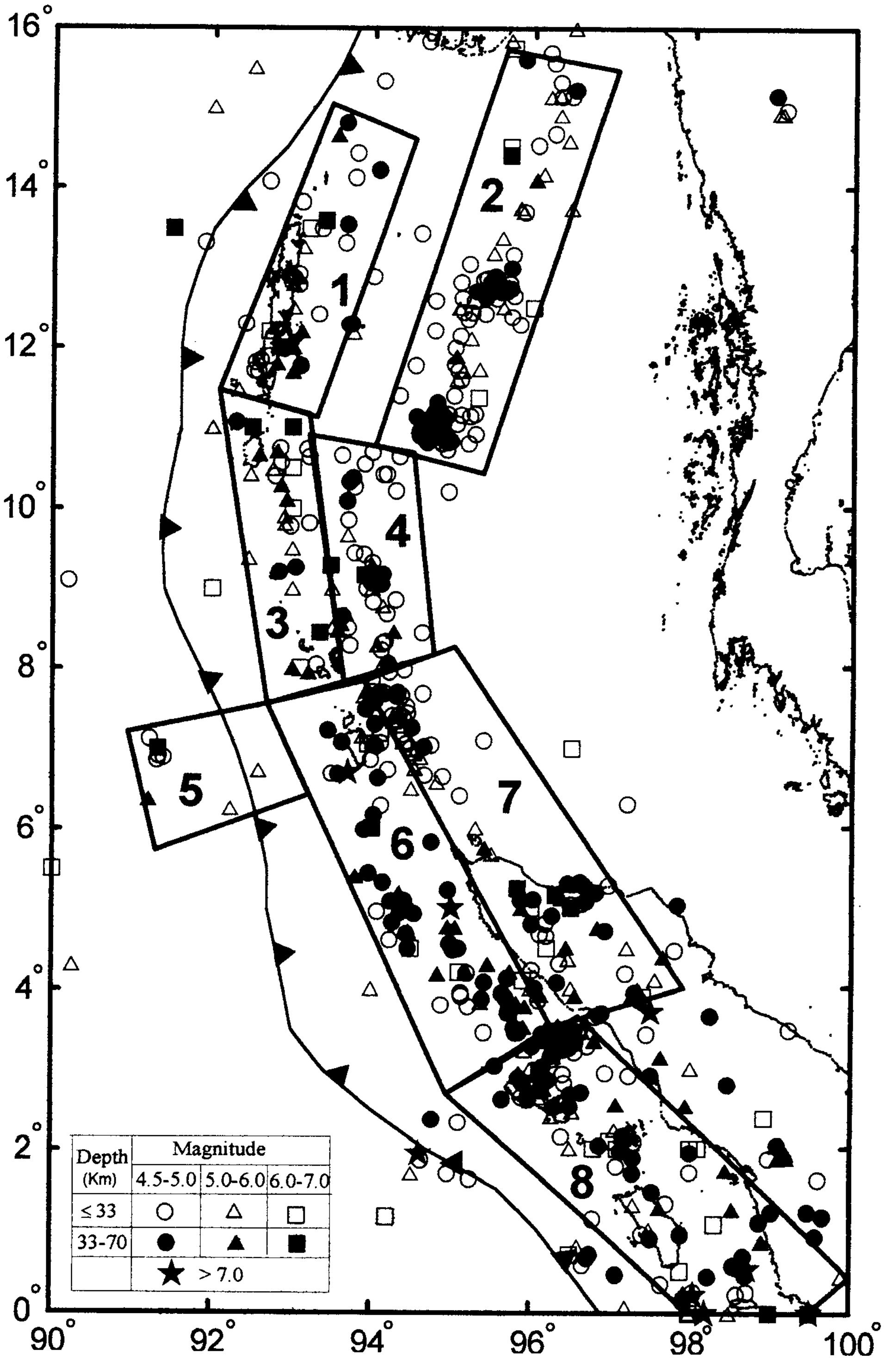

Figure 2. Seismicity map for the Andaman–west Sunda arc and adjacent region. Those events with h $\leq$ 70 km have been considered for the present study. The region is divided into 8 broad seismogenic sources as shown.

Table 1. Source parameters of available focal mechanism solutions in the Andaman–west Sunda arc and Andaman sea utilised in the present study. The classification of the faulting type is based on the calculation of mean slip angle given in Ravikumar et al. (1996). N – Normal, S – Strike-slip, T – Thrust. The solutions are compiled from: 1. Dasgupta and Mukhopadhyay (1993); 2. Fitch (1970); 3. Eguchi et al. (1979); 4. Fitch (1972); 5. Bergman and Solomon (1985); 6. Harvard CMT solutions

Sl. No.	Source	Date			Lat. °N	Long. °E	Depth Km	Mag. Ms	Seismic moment ($\times 10^{24}$)	Strike	Dip	Slip	Type of faulting	Ref.
1	7	1964	4	2	5.75	95.42	65			330	86	0	S	4
2	7	1964	4	3	3.91	96.56	51			290	70	–88	N	4
3	2	1967	2	14	13.75	96.47	13			60	55	–89	N	3
4	7	1967	4	12	5.32	96.45	63			278	28	92	T	4
5	7	1967	4	22	5.12	96.39	25			316	64	38	S	1
6	4	1967	7	2	8.65	93.59	44			351	75	–180	S	3
7	2	1967	7	28	14.17	96.12	22			80	56	–119	N	2
8	6	1967	8	21	3.72	95.74	40			293	12	88	T	4
9	1	1967	9	6	14.65	93.55	36			16	76	–89	N	2
10	4	1968	7	19	8.86	93.67	69			344	84	–11	S	1
11	3	1970	5	6	9.81	92.91	32	5.1		330	80	–89	N	1
12	8	1971	2	4	0.53	98.72	40	7.1		358	76	20	S	1
13	2	1971	3	28	12.12	95.22	22	6.3		360	90	3	S	3
14	2	1971	3	29	11.16	95.11	17			8	81	14	S	3
15	3	1971	6	5	9.38	92.46	25	5.2		333	80	–89	N	1
16	2	1971	8	12	12.50	95.08	20	5.1		348	88	–18	S	3
17	3	1971	11	5	10.11	92.93	53			360	20	73	T	1
18	3	1972	2	22	10.42	92.48	4			22	80	–28	S	1
19	3	1972	4	21	10.29	92.86	52			355	30	57	T	1
20	2	1972	11	13	12.20	95.30	24	5.5		346	86	–17	S	3
21	3	1973	7	9	10.66	92.59	44	5.2		315	86	25	S	3
22	5	1973	4	7	7.00	91.32	39	6.6		34	84	–4	S	5
23	6	1973	11	9	5.98	93.90	44			321	82	73	T	1
24	1	1974	2	16	11.47	92.32	20	6.0		10	10	41	T	1
25	7	1975	12	17	5.25	95.83	40	6.2		307	86	150	S	1
26	6	1976	11	3	4.22	95.19	1			330	74	48	S	1
27	6	1976	12	11	7.65	93.90	8	5.9		335	90	11	S	1
28	6	1977	5	25	4.20	95.74	67		410	78	19	–140	N	6
29	4	1977	10	13	9.43	93.90	21			344	76	–29	S	1
30	6	1977	12	3	3.52	95.91	22	5.9	14.0	87	50	–176	S	6
31	1	1978	2	7	12.80	92.99	3	5.3	3.10	129	43	46	T	6
32	1	1978	2	7	12.88	93.04	17		4.50	162	36	95	T	6
33	6	1978	6	7	6.29	94.11	25	4.5	0.63	275	68	16	T	6
34	2	1978	10	24	14.58	96.43	3		1.20	176	90	180	S	6
35	7	1979	3	16	5.19	96.32	49	5.8	7.30	249	32	48	T	6
36	1	1979	7	5	11.98	92.88	54			30	38	42	T	1
37	5	1979	10	16	6.37	91.20	38	5.1	2.40	14	76	–7	S	6
38	5	1980	2	19	6.72	92.58	2	5.2	4.40	308	35	38	T	6
39	7	1980	4	1	4.10	97.55	24		15.0	72	80	5	S	6
40	8	1980	12	30	0.06	97.20	11	5.4	2.40	286	27	31	T	6
41	1	1981	11	2	12.17	92.87	24	5.5	4.50	109	21	50	T	6
42	6	1982	1	20	7.05	93.95	16	6.3	29.0	87	69	9	S	6
43	6	1982	1	20	7.15	93.87	25	6.2	19.0	1	77	172	S	6
44	7	1982	2	24	4.38	97.65	50	5.4	7.15	300	49	51	T	6

Table 1. Continued

Sl. No.	Source	Date			Lat. °N	Long. °E	Depth Km	Mag. Ms	Seismic moment ($\times 10^{24}$)	Strike	Dip	Slip	Type of faulting	Ref.
45	6	1982	4	8	7.49	93.92	44	4.9		305	75	54	S	1
46	6	1982	5	22	7.54	93.92	35	5.3	2.25	19	21	–98	N	6
47	8	1982	10	31	2.92	96.06	48		1.30	299	51	–144	S	6
48	1	1982	12	16	11.69	92.99	60	4.6	2.87	286	52	30	S	6
49	6	1983	3	16	3.51	95.80	42			342	45	–150	S	1
50	3	1983	9	17	7.94	93.20	58		0.67	199	43	–43	N	6
51	6	1983	9	17	4.76	95.05	67		14.70	182	45	–25	S	6
52	2	1984	4	13	11.89	95.04	40	6.0	7.26	223	31	–90	N	6
53	2	1984	7	5	11.27	94.76	58		0.93	239	30	–109	N	6
54	2	1984	7	8	11.18	94.70	47	5.1	0.53	94	84	–36	S	6
55	2	1984	7	8	11.07	94.79	12		0.62	231	31	–126	N	6
56	2	1984	7	9	10.90	94.67	18	5.0	1.40	254	27	–83	N	6
57	2	1984	7	9	10.89	94.79	10		1.64	236	15	–108	N	6
58	2	1984	7	10	10.92	94.61	19	5.0	2.10	237	21	–109	N	6
59	2	1984	7	10	10.90	94.58	25		1.11	234	17	–114	N	6
60	2	1984	7	11	11.01	94.57	35	5.1	1.18	246	19	–84	N	6
61	2	1984	7	19	10.92	94.81	38	4.3	0.21	96	47	–58	N	6
62	2	1984	7	20	10.89	94.81	23		0.41	232	28	–110	N	6
63	2	1984	7	23	10.94	94.70	25		0.43	251	17	–95	N	6
64	2	1985	4	4	11.40	95.01	18	4.7	1.03	349	40	–179	S	6
65	6	1986	4	29	4.47	95.02	49	4.9	1.00	61	43	29	S	6
66	2	1986	6	29	15.15	96.32	23	5.1	2.30	242	17	–78	N	6
67	2	1986	8	7	11.72	95.35	24		0.46	173	82	172	S	6
68	7	1986	9	8	4.50	96.44	44	5.1	1.40	118	68	116	S	6
69	6	1987	10	14	4.07	95.41	66	4.7	40.00	191	71	0	S	6
70	6	1988	4	3	4.71	94.46	36	5.7	7.30	141	36	130	T	6
71	7	1989	5	3	6.97	94.58	32	4.8	0.62	56	49	–2	S	6
72	7	1989	7	30	4.79	96.00	41	4.8	0.93	309	62	117	S	6
73	8	1989	8	2	2.79	96.14	33		1.20	345	28	126	T	6
74	6	1990	4	30	7.33	94.27	26	5.2	2.50	332	73	–178	S	6
75	6	1990	7	31	3.86	95.39	37	4.6	0.47	171	38	125	T	6
76	6	1990	8	18	7.56	93.99	38	6.0	12.00	185	73	180	S	6
77	7	1990	11	15	3.89	97.40	29	6.8	120.0	226	71	78	S	6
78	7	1990	11	18	3.85	97.35	64		0.53	85	51	41	S	6
79	4	1990	12	29	8.28	94.06	16	6.0	15.0	347	86	179	S	6
80	8	1991	1	6	0.59	98.11	57	4.9	1.30	307	29	91	T	6
81	6	1991	3	8	7.23	93.44	53		0.90	219	43	0	S	6
82	2	1991	4	1	15.74	95.73	15	6.1	10.0	13	87	–180	S	6
83	2	1991	6	9	12.62	95.11	24	5.0	1.80	17	87	180	S	6
84	2	1991	6	12	14.89	96.32	10	5.2	0.66	99	80	–7	S	6
85	4	1991	7	18	8.22	94.11	27	5.0	2.10	73	81	1	S	6
86	6	1991	7	23	3.77	95.93	47	5.1	3.30	132	13	–38	N	6
87	6	1991	8	6	3.82	95.37	18	5.3	3.70	120	44	86	T	6
88	7	1991	8	26	6.93	94.53	26	5.6	5.20	56	72	8	S	6
89	7	1991	8	26	6.88	94.60	22	5.8	7.70	327	71	–168	S	6
90	7	1991	8	26	6.66	94.66	33	4.7	1.00	317	59	170	S	6
91	3	1992	3	17	9.21	92.83	67		0.51	227	71	1	S	6
92	2	1993	4	18	11.99	95.02	24	4.6	0.69	194	48	–143	S	6

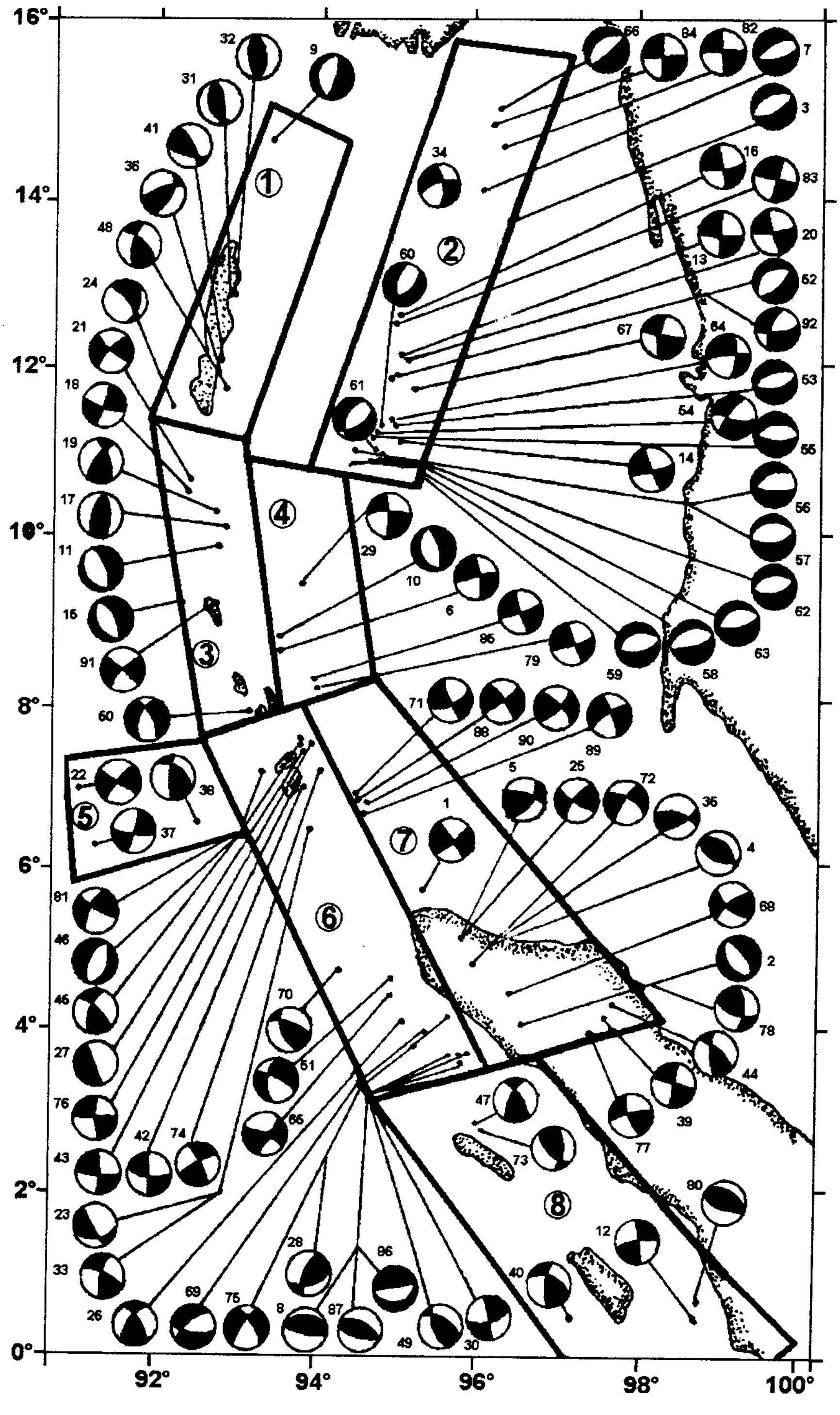

Figure 3. Map showing the 92 focal mechanism solutions used for identifying the broad seismogenic sources in the region. The numbers of solutions are as indicated in Table 1.

Table 2. Parameters used in the calculation of deformation for each seismogenic source identified in the region. L_1 and L_2 are length and width of the source. Az – azimuth of each deforming area. $M_{s,max}$ – maximum magnitude ever observed in each source for the complete data. a and b – are annual a and b value of the Gutenberg – Richter relation obtained based on the method of Milne and Davenport (1969) with errors in their estimate. t and M_{min} refer to data completeness for each source as described in the text

Source No.	L1 (Km)	L2 (Km)	t	M_{min}	Azimuth (° N)	a	b	Total no. of events	$M_{s,max}$	No. of events (Ms ≥ 6.0)	Mo × 10^{24} dyne cm/yr
1	416.0	129.1	1941	5.8	15	3.46 ± 0.11	0.75 ± 0.04	37	6.7	8	7.63
			1964	4.5							
2	573.9	153.0	1922	6.0	20	5.50 ± 0.05	1.10 ± 0.02	126	6.7	7	7.08
			1964	4.5							
3	401.7	105.2	1925	5.5	173	3.32 ± 0.08	0.72 ± 0.03	34	6.8	8	10.10
			1970	4.5							
4	306.1	133.9	1965	4.5	172	4.33 ± 0.10	0.93 ± 0.04	45	6.1	2	2.19
5	210.4	153.0	1973	4.5	70	1.28 ± 0.15	0.40 ± 0.06	8	6.6	1	5.90
6	535.6	143.4	1929	5.6	156	3.57 ± 0.05	0.71 ± 0.02	90	7.3	13	51.90
			1966	4.5							
7	545.2	153.0	1934	5.5	149	3.72 ± 0.07	0.76 ± 0.03	71	7.0	8	20.11
			1964	4.5							
8	526.1	172.1	1921	6.0	140	3.38 ± 0.06	0.66 ± 0.02	132	8.1	17	340.70
			1936	5.5							
			1964	4.6							

we calculated the value d (intercept) from the observed data. The magnitude–moment relation is shown in Figure 4 which gives a value of d = 16.09. This relation gives an r.m.s error of 0.17 with the observed data. Since the relation satisfactorily explains the observed data, we used it for converting the $M_{s,max}$ to $M_{o,max}$. The $M_{s,max}$ and the moment release rate $\dot{M}_O$ calculated for each source are also shown in Table 2.

Strain rates and deformation velocities

The strain rates and velocity tensor for each seismogenic source are calculated from the equations 1, 3–5 presented in section 2. The errors involved in this method were examined by Papazachos and Kiratzi (1992). They observed that the strain rates and velocity values are mainly controlled by errors in $\dot{M}_O$, while the directions of eigenvectors of deformation are mainly influenced by errors in $\bar{F}$. The uncertainties in the magnitude of observed velocities for each source are estimated through errors in $\dot{M}_O$ using the Monte-Carlo simulation method as outlined by Papazachos and Kiratzi (1992). It can be seen from eq.2 that errors in $\dot{M}_O$ are contributed from errors in a,b,c,d and $M_{s,max}$. For this purpose, the standard errors in a and b values given for each source in Table 2 are utilised. A value of 0.35 is assigned to the standard error in $M_{s,max}$. The error in c value is assumed to be 0.05 (Papazachos and Kiratzi, 1992) and the r.m.s. error of 0.17 in the fit of magnitude- moment relation is assigned to the standard error in d. Table 3 shows the components of strain rate tensor $\in$ and velocity tensor U and the eigensystem of velocity tensor with errors in eigenvalues for the 8 seismogenic sources in the region. The thickness of seismogenic layer is considered as l_3 = 40 km (for sources 1,3,6,8), l_3 = 30 km (for sources 2,4,5) and l_3 = 25 km (for source 7) based on the previous investigations on the crustal studies in the region (Kieckhefer et al., 1980; Mukhopadhyay, 1988).

Distribution of apparent stresses

Since apparent stresses characterise the static stress conditions, we studied the spatial variations of apparent stresses in the region. The apparent stresses are calculated as following:

$$\eta\sigma = \frac{\mu E_s}{M_O} \tag{7}$$

The apparent stress is a product of the average shear stress on the fault before and after faulting and an unknown seismic efficiency factor η, μ the rigidity mod-

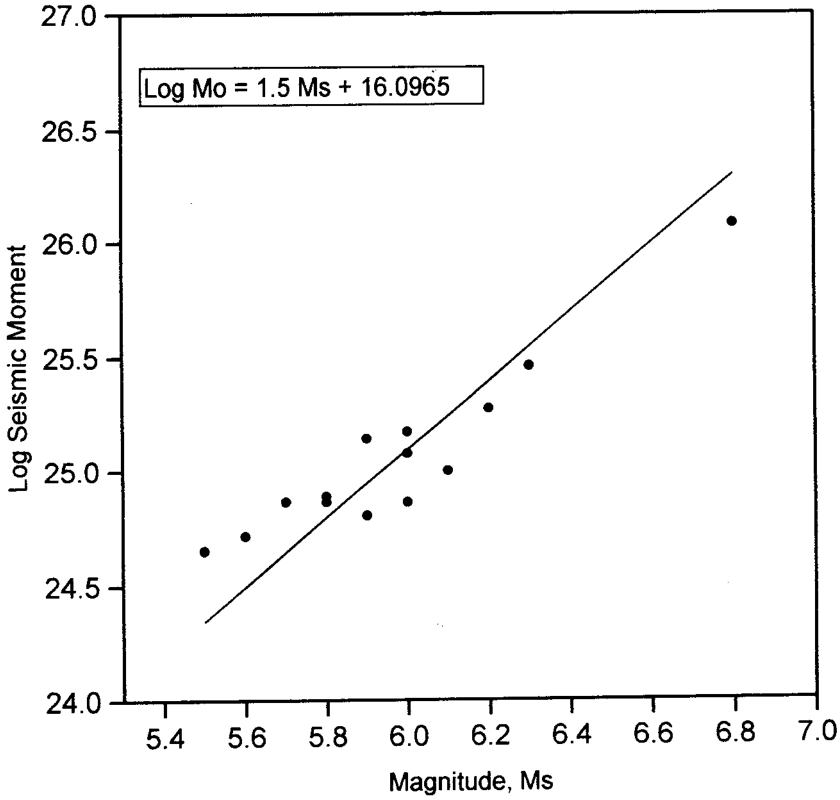

Figure 4. Plot showing the relation between the surface wave magnitude and seismic moments of large shallow earthquakes in the region. See text for more details.

Table 3. Components of the strain rate $\dot{\in}$ ($\times$ 10^{-7}/yr), velocity tensor **U** (mm/yr) and eigensystem of the velocity tensor for the 8 seismogenic sources in the region. Positive eigenvalues indicate tension while negative values indicate compression. Positive and negative plunge indicate that the eigenvector points into or out of the solid earth respectively

Source	Elements of the strain rate tensor $\dot{\in}$ (10^{-7}/yr)						Elements of the velocity tensor U (mm/yr)					
	11	12	13	22	23	33	11	12	13	22	23	33
1	–0.006	–0.005	0.001	–0.003	0.004	0.009	–0.287	–0.161	0.010	–0.072	0.034	0.036
2	0.019	–0.013	–0.015	0.000	0.004	–0.019	0.740	–0.281	–0.089	–0.110	0.023	–0.057
3	–0.011	–0.008	0.002	–0.004	0.007	0.015	–0.381	–0.145	0.018	–0.028	0.058	0.060
4	–0.002	–0.006	0.001	0.003	0.003	–0.002	–0.049	–0.164	0.006	0.069	0.016	–0.005
5	–0.044	0.028	–0.021	0.026	0.023	0.017	–0.657	0.472	–0.125	0.600	0.139	0.052
6	–0.030	–0.023	0.006	–0.012	0.020	0.042	–0.975	–0.398	0.049	–0.009	0.161	0.168
7	–0.081	–0.009	0.004	0.052	–0.010	0.030	–3.193	0.068	0.019	1.242	–0.051	0.075
8	–0.166	–0.129	0.035	–0.070	0.113	0.236	–4.031	–2.445	0.277	–0.006	0.906	0.945

Table 3. Continued

Source	Eigensystem of the velocity tensor (mm/yr)								
	λ_1	Az°	Pl°	λ_2	Az°	Pl°	λ_3	Az°	Pl°
1	–0.374 ± 0.037	28.4	3.6	–0.002 ± 0.00	120.6	32.6	0.053 ± 0.00	112.8	57.1
2	0.835 ± 0.052	343.3	–5.9	–0.195 ± 0.01	73.1	–1.4	–0.067 ± 0.00	329.4	–84.0
3	–0.436 ± 0.051	20.1	4.2	–0.009 ± 0.00	112.9	33.8	0.095 ± 0.01	103.9	55.9
4	–0.166 ± 0.014	35.2	4.9	0.185 ± 0.01	125.0	3.0	–0.004 ± 0.00	3.7	–84.0
5	–0.844 ± 0.122	341.0	–10.0	0.770 ± 0.11	72.3	7.5	0.069 ± 0.01	197.6	77.2
6	–1.126 ± 0.134	20.2	4.5	0.019 ± 0.00	114.1	–40.3	0.292 ± 0.03	105.0	49.3
7	–3.194 ± 0.295	359.1	0.3	1.246 ± 0.11	89.1	–2.5	0.073 ± 0.00	81.2	87.5
8	–5.252 ± 0.652	25.9	5.9	1.780 ± 0.22	110.6	42.0	0.379 ± 0.04	302.4	47.4

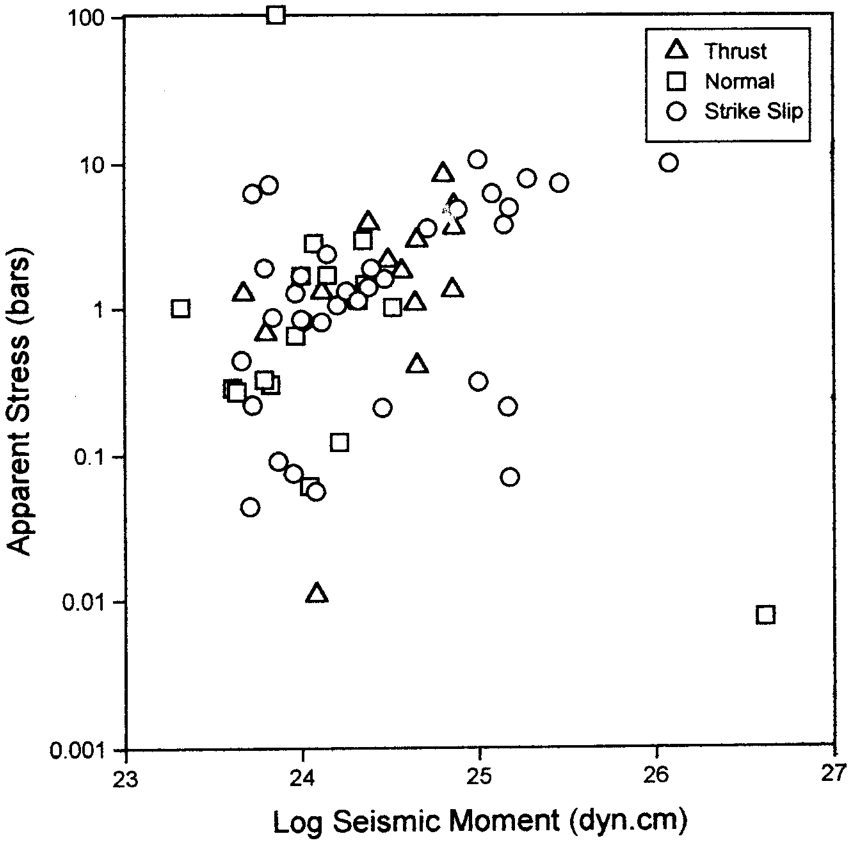

Figure 5. Shows variation of apparent stress with the fault type in the region. Note that mechanism type of events has no significant effect on the magnitude of apparent stresses.

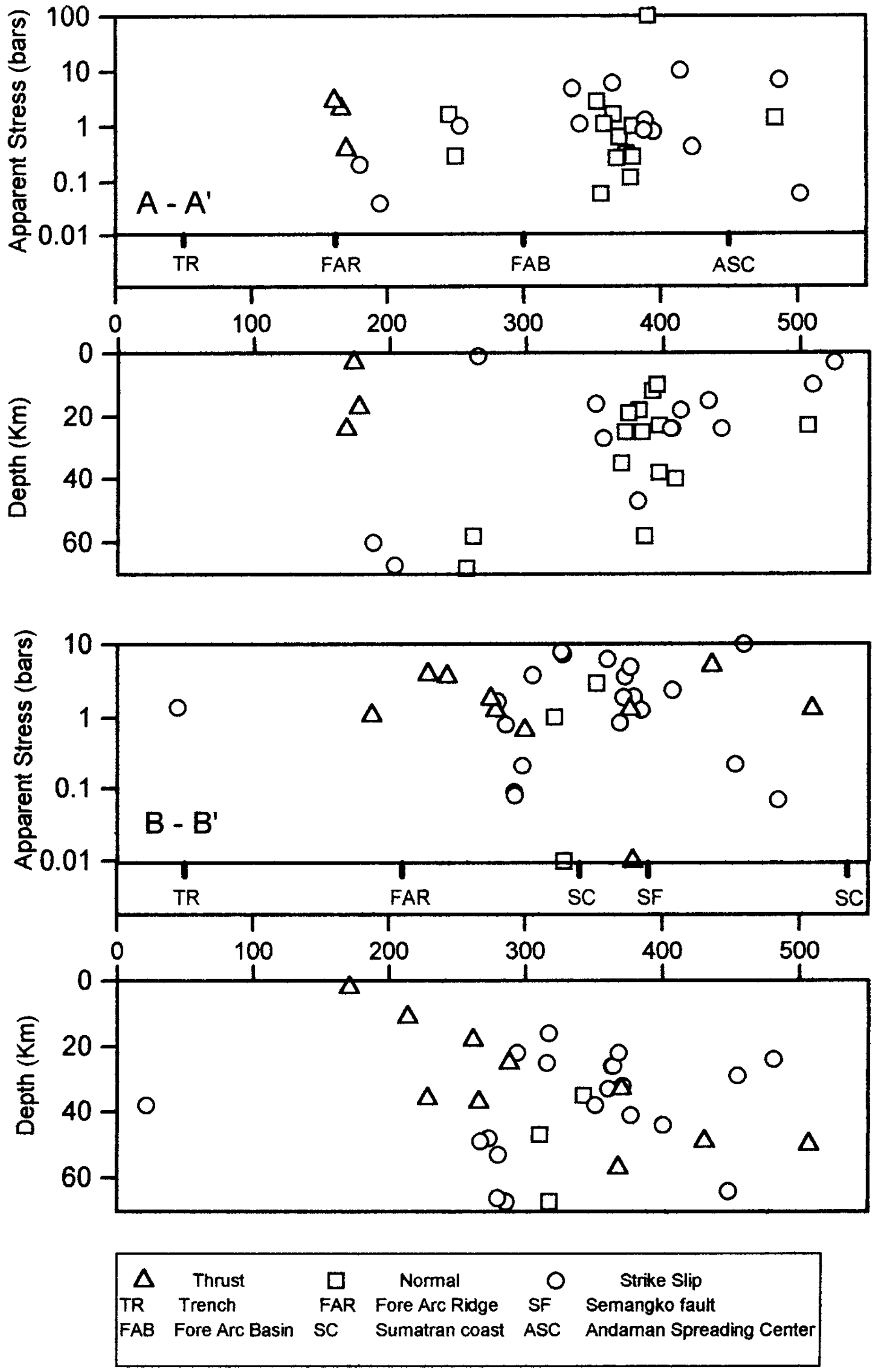

Figure 6. Distribution of apparent stresses across the shallow subduction zone in the northern and southern part of the study region. See Figure 1 for location of the sections.

ulus taken as 3.0×10^{11}dyn/cm^2 and E_s is energy of the earthquake. We calculated apparent stresses for all those events with seismic moments listed in Table 1. The energy-magnitude relation of Gutenberg-Richter (1956) i.e.,

$$\text{Log } E = 11.4 + 1.5M_s \tag{8}$$

is used for estimating energy of the event. Though, such an estimation of Ms is not straight forward since Es should represent the integral of the spectrum over the entire frequency band (Kanamori et al., 1993), this relation provide an internally consistent means for estimating Es when only relative variations in apparent stresses are desired rather than absolute apparent stress levels (Burr and Solomon, 1978). We classified the apparent stress data for various faulting type. Figure 5 shows the relation between apparent stresses and seismic moment for different faulting pattern. Except few events, all the values range between 0.1–10 bars. In general, the values increase with increasing seismic moment for all types of mechanisms. For a given size of earthquake, the difference in apparent stress values for different types of mechanisms are not significant. In order to study the spatial distribution of apparent stresses across the arc, we considered two east–west sections AA' and BB' (see Figure 1 for location). The events pertaining to sectors I and II are projected onto section AA' and those pertaining to III and IV are projected onto section BB' (Figure 1). Such a bifurcation is necessary because the arc significantly changes in orientation from south to north, and also the northern part of the study region is charecterised by active back arc spreading. The sections AA' and BB' are shown in Figure 6. The sections show that the thrust faulting events mostly observed in the fore arc region have similar apparent stresses when compared to normal and strike-slip events in the back arc region. No clear relation between the depth of faulting and the apparent stresses is observed from Figure 6.

Results and discussion

The results on the deformation pattern obtained for each source shown in Table 3 are presented diagrammatically in Figure 7. For a meaningful representation of horizontal plate velocities, only those eigen vectors with plunge ($< 15°$) are shown. Certain salient results on the deformation pattern for each seismogenic source are given below:

Andaman–Nicobar–Nias fore arc region (sources 1, 3, 6, 8)

A total of 42 focal mechanism solutions in this belt mostly showing thrust and strike-slip faulting are used in the moment tensor summation. The compressional deformation takes place in this belt in a mean direction of N 23° and the velocities show compression of 5.2 ± 0.65 mm/yr for source 8, 1.12 ± 0.13 mm/yr for source 6, decreasing to an average compression of 0.4 ± 0.04 mm/yr for sources 1 and 3.

Back arc spreading in the Andaman sea (source 2)

This region consists mostly of shallow events within the top part of the overriding plate. A total of 26 mechanisms showing both normal and strike-slip faulting are used in the moment tensor summation. While normal faulting events occur on the flanks of the spreading rift valley, strike-slip events are related to short transforms offsetting the spreading ridge segments. The eigen system of velocity tensor suggests extension of 0.83 ± 0.05 mm/yr along N343° and compression of 0.19 ± 0.01 mm/yr along N73°.

Nicobar Deep and west Andaman fault (source 4)

A total of 5 focal mechanism solutions showing mostly right-lateral slip are used in the moment tensor summation. The deformation velocities in this region suggests compression of 0.16 ± 0.01 mm/yr along N35° and extension of 0.18 ± 0.01 mm/yr along N125°.

Transverse seismic zone across the Andaman trench (source 5)

This source covers the region between 6° and 7° N across the Andaman trench. The region is charecterised by an E–W fault zone and has been correlated as a wide ridge / upper trench slope by Moore et al. (1980). The deformation velocities show compression of 0.84 ± 0.12 mm/yr along N341° and extension of 0.77 ± 0.11 mm/yr along N72°.

Semangko fault zone in northern Sumatra (source 7)

A total of 16 focal mechanism solutions are used in the moment tensor summation. Except few, all other solutions show right lateral faulting on steep dipping nodal planes. The eigen system of velocity tensor suggests N-S compression of 3.19 ± 0.29 mm/yr and an E–W extension of 1.24 ± 0.11 mm/yr.

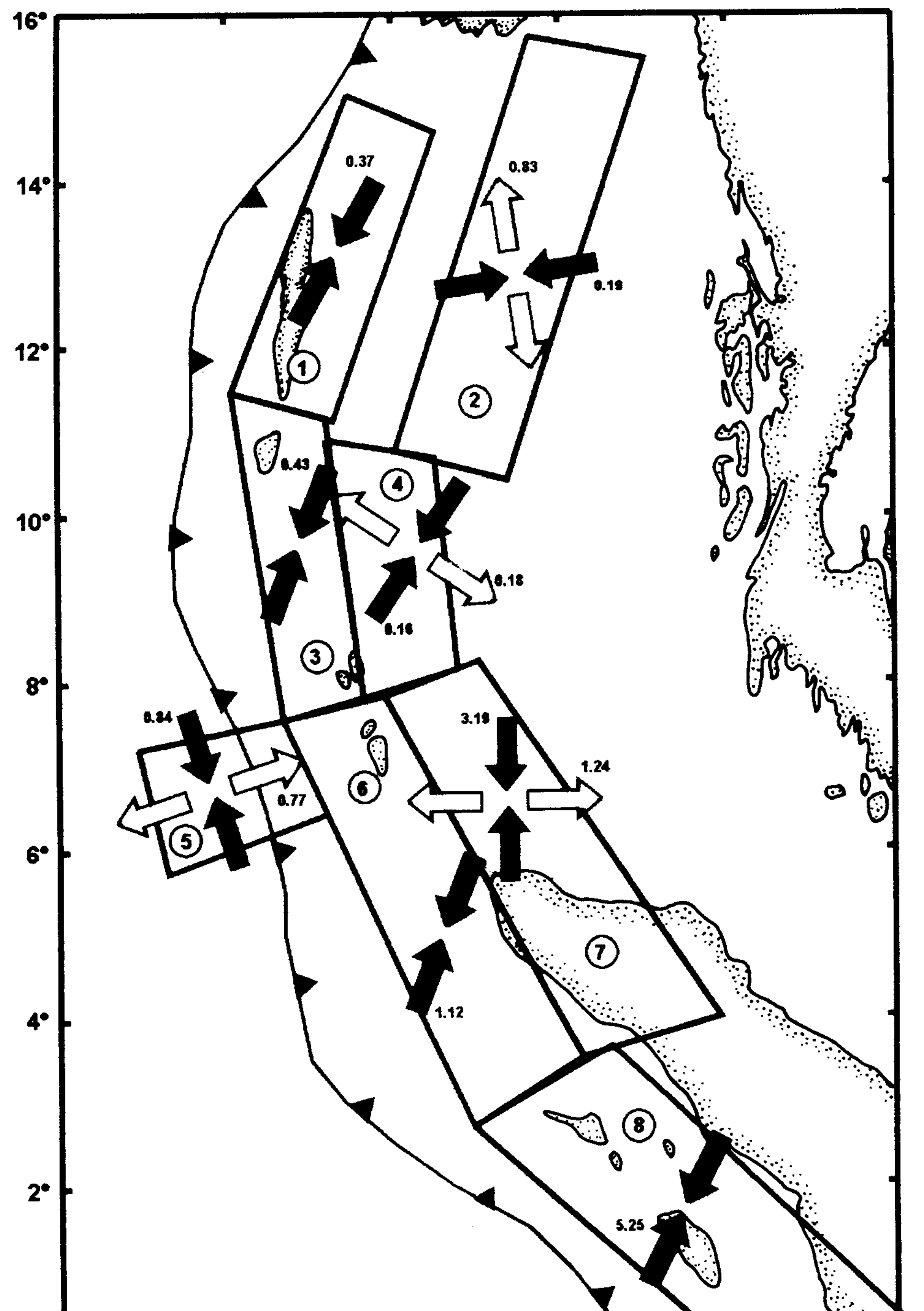

Figure 7. Distribution of deformation velocities for the 8 seismogenic sources identified in the present study. The values are in mm/yr. Converging arrows indicate compression while diverging arrows indicate extension. Only those eigen vectors with plunge $<15°$ are shown.

The above results are consistent with the overall tectonics of the region. The deformation pattern indicate the dominance of compressive stresses in the fore arc region with the direction of maximum compression in almost NNE-SSW. While, it is almost normal to the trench in the Sumatran fore arc near Nias island region, the compression takes more oblique trend with respect to the trench towards north near Andaman islands. Biswas et al. (1992) infer N–S shear stresses due to oblique subduction in the Andaman arc region. The compressional velocities decrease northward in the fore arc region charecterised by deficiency of moment release and absence of large magnitude earthquakes north of 8°N (Table 2). Geophysical data indicate that the 90°E ridge partially subducts below the Andaman trench (Curray et al., 1982; Mukhopadhyay, 1988; Mukhopadhyay and Krishna, 1995; Gopala Rao et al., 1997). Further, Dasgupta and Mukhopadhyay (1993) observed a contorted Benioff zone east of the Nicobar islands and inferred as the effect of ridge subduction. Such charecteristic changes in the seismicity pattern have been interpreted due to the buoyancy forces related to subduction of aseismic ridges (Vogt, 1973; Kelleher and McCann, 1976; Chung and Kanamori, 1978). The NW-SE extension of 0.80 mm/yr perpendicular to the Andaman spreading ridge and compression of 0.19 mm/yr in the direction of regional stress field conforms with the stress model inferred by Biswas et al. (1992) for the Andaman sea region. The events along the back arc spreading region also include an earthquake swarm of July 8, 1984 with most of the mechanisms reported by Dziewonski et al. (1983) showing dominantly normal faulting. Such a faulting pattern for swarms along the slow-spreading ridges indicate extensional tectonic activity (Bergman and Solomon, 1990; Radha Krishna and Arora, 1998). The vertical component of velocities indicate crustal thinning in the Andaman sea and crustal thickening all along the fore arc and Semangko fault region. The tensional stress regime in the Andaman sea gradually become compressional towards the fore arc and northern Sumatra. The results on apparent stresses do not indicate any significant variation with faulting type. Also, the stress levels remain uniform between the fore arc thrust region to back arc tensional zone in contrast to the general observation that thrust faulting events have 2 to 3 times higher apparent stress values than normal events in the shallow subduction zones (Cocco and Rovelli, 1989; Zobin, 1996). This discrepancy could be due to oblique plate subduction and active back arc spreading in the Andaman arc region which give rise to the absence of large fore arc thrust events and the overall dominance of tensional and strike-slip stresses in the overriding plate.

Conclusions

Shallow seismicity, focal mechanism data and other morphotectonic details in the Andaman–west Sunda arc and Andaman sea indicate that the region could be divided into 8 broad seismogenic sources of homogeneous deformation. The deformation velocities calculated for these identified sources show that while compressional stresses dominate the entire fore arc and the northern Sumatra region, tensional stresses prevail in the back arc spreading Andaman sea region. North of 8°N where the 90°E Ridge partially subducts below the arc, the fore arc region is charecterised by the deficiency of moment release and absence of large magnitude earthquakes. The apparent stresses estimated for selected events do not indicate any significant variation with faulting type and also the stress levels remain uniform both along and across the arc.It is inferred that the oblique plate convergence, partial subduction of the 90°E Ridge in north below Andaman trench and active back arc spreading in the Andaman sea are the main controlling factors for the observed stress field within the overriding plate in this region.

Acknowledgements

Financial assistance was made available to one of the authors (T.D.S) in the form of University Grants Commission fellowship.

References

Aki, K. and Richards, P., 1980, Quantitative Seismology, Theory and methods. Freeman, San Francisco, CA, 557 pp.

Bergman, E.A. and Solomon, S.C., 1985, Earthquake source mechanisms from body-waveform inversion and intraplate tectonics in the northern Indian Ocean, *Phys. Earth Planet. Inter.* **40**, 1–23.

Bergman, E.A. and Solomon, S.C., 1990, Earthquake swarms on the Mid-Atlantic Ridge, products of magmatism or extensional tectonics ? *J. Geophys. Res.* **95**, 4943–4965.

Biswas, S., Majumdar, R.K. and Dasgupta, A. 1992, Distribution of stress axes orientation in the Andaman–Nicobar island region, a possible stress model and its significance for extensional tectonics of the Andaman sea, *Phys. Earth Planet. Inter.* **70**, 57–63.

Burr, N.C. and Solomon, S.C., 1978, The relationship of source parameters of oceanic transform earthquakes to plate velocity and transform length, *J. Geophys. Res.* **83**, 1193–1205.

Chung, W.Y. and Kanamori, H., 1978, A mechanical model for plate deformation associated with aseismic ridge subduction in the New Hebrides arc, *Tectonophysics* **50**, 29–40.

Cocco, M. and Rovelli, A., 1989, Evidence for the variation of stress drop between normal and thrust faulting earthquakes in Italy, *J. Geophys. Res.* **94**, 9399–9416.

Curray, J.R., 1987, The Sunda arc, A model for oblique plate convergenge. In: Van Hinte, Tj., van Weering, C.E. and Fortruin, A.R. (eds), Proc. Symp. Snellius-II expedition, Jakarta, Nov. 23–28, 1987. Vol. 1 Geology and Geophysics of the Banda arc and adjacent areas, *Neth. J. Sea Res.*

Curray, J.R., Moore, D.G., Lawver, L., Emmel, F.J., Raith, R., Henry, M. and Kieckhefer, R., 1979, Tectonics of the Andaman sea and Burma, *Am. Assoc. Pet. Geol. Mem.* **29**, 189–198.

Curray, J.R., Emmel, F.J., Moore, D.G. and Raitt, R.W., 1982, Structure, tectonics and geological history of the northeastern Indian Ocean, In: Nairn, A.E.M. and Stehli, F.G. (eds), *The Ocean Basins and Margins,* Plenum, New York **Vol. 6**, 399–450.

Dasgupta, S., 1992, Seismotectonics and stress distribution in the Andaman plate, *Mem. Geol. Soc. Ind.* **23**, 319–334.

Dasgupta, S. and Mukhopadhyay, M., 1993, Seismicity and plate deformation below the Andaman arc, northeastern Indian Ocean, *Tectonophysics* **225**, 529–542.

Dziewonski, A.M., Friedman, A., Giardini, D. and Woodhouse, J.H., 1983, Global seismicity of 1982, Centroid moment tensor solutions for 308 earthquakes, *Phys. Earth Planet. Inter.* **33**, 76–90.

Eguchi, T., Uyeda, S. and Maki, T., 1979, Seismotectonics and tectonic history of the Andaman sea, *Tectonophysics* **57**, 35–51.

Fitch, T.J., 1970, Earthquake mechanisms in the Himalaya, Burmese and Andaman regions and Continental tectonics in Central Asia, *J. Geophys. Res.* **75**, 2699–2709.

Fitch, T.J., 1972, Plate convergence, transcurrent faults and internal deformation adjacent to southeast Asia and the western Pacific, *J. Geophys. Res.* **77**, 4432–4460.

Geller, R.J. and Kanamori, H. 1977, Magnitudes of great shallow earthquakes from 1902 to 1952, *Bull. Seis. Soc. Am.* **67**, 587–598.

Gopala Rao, D., Krishna, K.S. and Sar, D., 1997, Crustal evolution and sedimentary history of the Bay of Bengal since the Cretaceous, *J. Geophys. Res.* **102**, 17747–17768.

Gutenberg, G. and Richter, C.F., 1954, *Seismicity of the Earth and Its Associated Phenomena*, Princeton Univ. Press, Princeton, N.J., 310 pp.

Gutenberg, G. and Richter, C.F., 1956, Earthquake magnitude, intensity, energy and accelaration, *Bull. Seis. Soc. Am.* **46**, 105–145.

Jackson, J. and McKenzie, D.P. 1988, The relationship between plate motion and seismic moment tensors, and the rates of active deformation in the Mediterranean and middle east, *Geophys. J.* **93**, 45–73.

Kanamori, H. and Anderson, D. 1975, Theoretical basis of empirical relations in seismology, *Bull. Seis. Soc. Am.* **65**, 1073–1095.

Kanamori, H., Mori, J., Hauksson, E., Heaton, T.H., Hutton, L.K. and Jones, L.M., 1993, Determination of earthquake energy release and M_L using Terrascope, *Bull. Seis. Soc. Am.* **83**, 330–365.

Kelleher, J. and McCann, W. 1976, Buoyant zones, great earthquakes, and unstable boundaries of subduction, *J. Geophys. Res.* **81**, 4885–4896.

Kieckhefer, R.M., Shor, G.G. Jr. and Curray, J.R., 1980, Seismic refraction studies of the Sunda trench and fore arc basin, *J. Geophys. Res.* **85**, 863–889.

Kiratzi, A., 1993, A study on the active crustal deformation of the north and east Anatolian fault zones, *Tectonophys.* **218**, 375–381.

Kiratzi, A. and Papazachos, C.B., 1995, Active crustal deformation from the Azores triple junction to the middle east, *Tectonophys.* **243**, 1–24.

Kostrov, V.V., 1974, Seismic moment and energy of earthquakes and seismic flow of rocks, *Izv. Acad. Sci., USSR. Phys. Solid Earth.* **1**, 23–44.

Maung, H., 1987, Transcurrent movements in the Burma–Andaman sea region, *Geology* **15**, 911–912.

Milne, W. and Davenport, A., 1969, Determination of earthquake risk in Canada, *Bull. Seis. Soc. Am* **59**, 729–754.

Molnar, P., 1979, Earthquake recurrence intervals and plate tectonics, *Bull. Seis. Soc. Am.* **69**, 115–133.

Moore, G.F. and Curray, J.R., 1980, Structure of the Sunda trench lower slope off Sumatra from multichannel seismic reflection data, *Mar. Geophys. Res.* **4**, 319–340.

Moore, G.F. and Karig, D.E., 1980, Structural geology of Nias island, Indonesia, implications for subduction zone tectonics, *Am. J. Seismol.* **280**, 193–223.

Moore, G.F., Curray, J.R., Moore, D.G. and Karig, D.E., 1980, Variations in geologic structure along the Sunda fore arc, NE Indian Ocean. In: Hayes, D.E. (ed.), The Tectonic and Geologic Evolution of SE Asian Seas and Islands, *Am. Geophys. Un. Monogr.* **23**, 145–160.

Mukhopadhyay, M., 1984, Seismotectonics of subduction and back arc rifting under the Andaman sea, *Tectonophysics* **108**, 229–239.

Mukhopadhyay, M., 1988, Gravity anomalies and deep structure of the Andaman arc, *Mar. Geophys. Res.* **9**, 197–210.

Mukhopadhyay, M. and Krishna, M.R., 1995, Gravity anomalies and deep structure of the Ninety east Ridge north of the equator, eastern Indian Ocean – A hot spot trace model, *Mar. Geophys. Res.* **17**, 201–216.

Papazachos, B.C. 1990, Seismicity of the Aegean and surrounding area, *Tectonophysics* **178**, 287–308.

Papazachos, C.B. and Kiratzi, A., 1992, A formulation for reliable estimation of active crustal deformation and its application to central Greece, *Geophys. J. Int.* **111**, 424–432.

Papazachos, C.B. and Kiratzi, A., 1996, A detailed study of the active crustal deformation in the Aegean and surrounding area, *Tectonophysics* **253**, 129–153.

Papazachos, C.B., Kiratzi, A. and Papazachos, B., 1992, Rates of active crustal deformation in the Aegean and the surrounding area, *J. Geodynamics* **16**, 147–179.

Radha Krishna, M. and Arora, S.K., 1998, Space-time seismicity and earthquake swarms, certain observations along the slow-spreading mid-Indian ocean ridges, *Proc. Ind. Acad. Sci. (EPS)* **107**, 161–173.

Rajendran, K. and Gupta, H.K., 1989, Seismicity and tectonic stress field of a part of the Burma–Andaman–Nicobar arc, *Bull. Seis. Soc. Am.* **79**, 989–1005.

Ravikumar, M., Rao, N.P. and Chalam, S.V., 1996, A seismotectonic study of the Burma and Andaman arc regions using centroid moment tensor data, *Tectonophysics* **253**, 155–165.

Rodolfo, K.S., 1969, Bathymetry and marine geology of the Andaman basin and its tectonic implications for SE Asia, *Am. Assoc. Pet. Geol. Bull.* **52**, 2422–2437.

Rothe, J.P., 1969, *The Seismicity of the Earth,* UNESCO, Paris, 336 pp.

Sinhval, H., Khattri, K.N., Rai, K. and Gaur, V.K., 1978, Tectonics and time space seismicity of the Andaman Nicobar region, *Bull. Seis. Soc. Am.* **68**, 399–409.

Surender Kumar, 1981, Geodynamics of Burma and Andaman–Nicobar region on the basis of tectonic stresses and regional seismicity, *Tectonophysics* **79**, 75–95.

Uyeda, S. and Kanamori, H., 1979, Back arc opening and the mode of subduction, *J. Geophys. Res.* **84**, 1049–1061.

Verma, R.K., Mukhopadhyay and Bhuin, N.C., 1978, Seismicity, gravity and tectonics in the Andaman sea, *J. Phys. Earth* **26**, 233–248.

Vogt, P.R., 1973, Subduction and aseismic ridges, *Nature* **241**, 189–191.

Weeks, L.A., Harbison, R.A. and Peter, G., 1967, Island arc system in Andaman sea, *Am. Assoc. Pet. Geol. Bull.* **51**, 1803–1815.

Zobin, V.M., 1996, Apparent stress of earthquakes within the shallow subduction zone near Kamchatka Peninsula, *Bull. Seis. Soc. Am.* **86**, 811–820.